

X-ray crystal structure analysis and the Ru valence of $\text{Ba}_4\text{Ru}_3\text{O}_{10}$ single crystals

Taichi Igarashi^{1,*}, Yoshio Nogami^{2,†}, Yannick Klein³, Gwenaëlle Rousse³,

Ryuji Okazaki¹, Hiroki Taniguchi¹, Yukio Yasui⁴, and Ichiro Terasaki¹

¹*Department of Physics, Nagoya University, Nagoya 464-8602, Japan*

²*Department of Physics, Okayama University, Okayama 700-8530, Japan*

³*Université Pierre et Marie Curie-Paris 6, IMPMC-CNRS UMR 7590 Campus Jussieu, 4 place Jussieu F-75252 Paris Cedex 05, France and*

⁴*Department of Physics, Meiji University, Kawasaki 214-8571, Japan*

We present the single-crystalline x-ray diffraction study on the $\text{Ba}_4\text{Ru}_3\text{O}_{10}$ consisting of the corner-shared Ru_3O_{12} trimers. The crystal structure is re-determined from 78 to 300 K across an antiferromagnetic transition at 105 K. The orthorhombic symmetry ($Cmca$, space group No. 64) is preserved at all temperatures measured. This structure presents exceptionally long Ru-O distances characterized by a significant distribution within the Ru_3O_{12} trimer. A bond valence sum calculation suggests that the charge disproportionation within the Ru_3O_{12} trimer emerges even at room temperature, which we ascribe to molecular orbital formation in the Ru_3O_{12} trimer, as supported by recent theoretical calculations. Based on the analyzed crystal structure, the electronic states and the nature of the phase transition at 105 K are discussed.

PACS numbers:

I. INTRODUCTION

Ruthenium oxides including tetravalent Ru ions exhibit various fascinating electronic and magnetic states owing to the multiple degrees of freedom of $4d$ electrons as seen in complex electronic phase diagrams of ARuO_3 and A_2RuO_4 ($A = \text{Ca}, \text{Sr}$). In $\text{Ca}_{2-x}\text{Sr}_x\text{RuO}_4$, for instance, the ground state varies from an antiferromagnetic insulating¹ ($x < 0.2$) to a superconducting phase² ($x = 2$) through a spin-glass state in the wide composition range.³ Structurally, these compounds belong to the Ruddlesden-Popper phases where the RuO_6 octahedra are corner-shared. In contrast, when Ba^{2+} is combined with Ru^{4+} , the ruthenates derive from the hexagonal perovskite-type structure. An important feature in the hexagonal ruthenates is that the RuO_6 octahedra are face-shared, leading to a shorter Ru-Ru distance than in Ru metal. This indicates a stronger hybridization of the Ru $4d$ orbitals and the resulting molecular orbital formation may introduce an additional internal charge degree of freedom in such Ru multimer, which can be an origin for exotic electronic properties in this system.

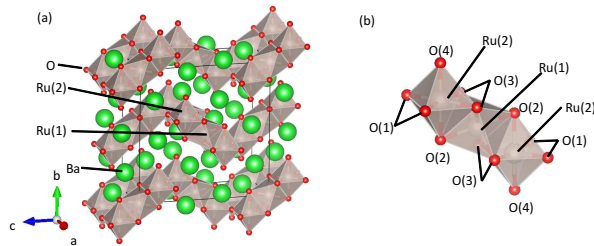


FIG. 1: (Color online) (a) The crystal structure of $\text{Ba}_4\text{Ru}_3\text{O}_{10}$. (b) Ru_3O_{12} trimer in $\text{Ba}_4\text{Ru}_3\text{O}_{10}$.

The barium ruthenate $\text{Ba}_4\text{Ru}_3\text{O}_{10}$ with tetravalent Ru ions⁴ is related to the hexagonal-perovskite 9R-BaRuO_3 in which Ru_3O_{12} trimers made of face shared RuO_6 octahedra. While in the latter compound, each trimer is connected with

six neighboring trimers via the corners of the outer RuO_6 octahedra, the number of connections is limited to four in $\text{Ba}_4\text{Ru}_3\text{O}_{10}$, and This compound corrugated layers stacked along the b axis [Fig. 1(a)]. Each trimer is built upon two inequivalent Ru sites, where the center and outer Ru ions are denoted as Ru(1) and Ru(2), respectively [Fig. 1(b)]. The structure was reported to be orthorhombic with space group $Cmca$ (No.64) at room temperature by Carim *et al.*,⁵ and no symmetry lowering was detected down to 10 K in a neutron powder diffraction experiment by Klein *et al.*⁶ An intriguing feature in $\text{Ba}_4\text{Ru}_3\text{O}_{10}$ is an unusual phase transition at $T_N = 105$ K, below which an antiferromagnetic order develops with an opening of an energy gap in the charge transport phenomena.⁶ This antiferromagnetic order is unique in the sense that it does not break the translational symmetry of the lattice, but is characterized by a sudden drop from the susceptibility experiment. Moreover, neutron powder diffraction patterns indicate the growth of magnetic intensity on the nuclear (0 0 2) reflection below T_N .

Here we present the synthesis and x-ray structural analysis of $\text{Ba}_4\text{Ru}_3\text{O}_{10}$ single crystals in a wide temperature range from 78 to 300 K with a reliability factor (R -factor) better than 2%. All the low-temperature studies of the title compound reported thus far were done with polycrystalline samples. Owing to the complicated structure, the Rietveld refinements do not give satisfactory reliability factors. In contrast, single crystal structure analysis can make full use of all the Bragg reflections on the Ewald sphere, and the structure can be solved with a model-free approach. We have confirmed the space group to be $Cmca$ using extinction rule at all temperatures above 78 K, and have found no additional superlattice reflections below T_N , which indicates no structural symmetry breaking in this transition. On the basis of the determined structure, we have further found that some bond lengths are anomalously long, which exhibit substantial temperature dependence. Using a bond valence sum calculation, we evaluate the formal valences of Ru(1) and Ru(2) as a function of temperature, and discuss the electronic states and the nature of the 105 K transition.

II. EXPERIMENTS

Single crystals of $\text{Ba}_4\text{Ru}_3\text{O}_{10}$ were synthesized from stoichiometric mixture of BaCO_3 (99.9%) and RuO_2 (99.9%) using a solid state reaction. The starting materials were mixed in an agate mortar with a pestle, and heated in an alumina crucible at 1000°C for 12 h in air. The obtained powder was mixed and heated again at 1200°C for 24 h in air. The powder was then reground, pressed into pellets, and heated at 1400°C for 24 h in air. The pellets were annealed at 1400°C for 192 h, and small single crystalline samples were grown on the surface of the pellets.

In order to determine the crystal structure precisely we measured two samples (Sample1 and Sample2) in different conditions. The dimensions of Sample1 and Sample2 were approximately $40 \times 50 \times 150 \mu\text{m}^3$ and $50 \times 60 \times 160 \mu\text{m}^3$, respectively. Sample1 was used to determine the space group and the unit cell parameters from 300 down to 78 K. The structural determination was carried out with an automated RIGAKU Saturn Varimax system equipped with CCD detector. The instrument employed $\text{MoK}\alpha$ radiation at 50 kV and 24 mA using a doubly focused mirror. The sample stage was controlled by a triaxial rotation system (ω, χ, ϕ) equipped with $1/4 \chi$. Sample1 was measured with the oscillation method, where the rotation parameters were fixed to $2\theta = 20^\circ$, $\chi = 45^\circ$, and $\phi = 0^\circ$, and ω was swept from 0 to 180° with an oscillation angle $\delta = 0.5^\circ$ during a counting time of 1 s. Sample2 was also measured by the oscillation method, but the measurement was expanded to 4-times larger range on the Ewald sphere to determine the atomic coordinates more precisely. Specifically, ω was swept from 0 to 180° under the conditions of $(2\theta, \phi) = (20^\circ, 0^\circ)$, $(20^\circ, 90^\circ)$, $(70^\circ, 180^\circ)$, and $(70^\circ, 270^\circ)$. The temperature was controlled with spraying nitrogen gas, and was monitored at the outlet of the gas. We use this temperature throughout the present manuscript, which is approximately 3 K lower than the sample temperature. The space group and the lattice constants were computationally determined with Crystal Clear, RIGAKU, and the integrated intensity for all the reflections was calculated simultaneously. The crystal structure was determined from the obtained reflection intensity using a direct method with SHELX-97⁷ and Yadokari-XG 2009.⁸

III. RESULTS AND DISCUSSION

From a careful investigation of the Laue symmetry and the extinction rule, the structural symmetry at 300 K is determined to be orthorhombic ($Cmca$), with lattice parameters of $a = 5.7740(5) \text{ \AA}$, $b = 13.2571(10) \text{ \AA}$, and $c = 13.0649(9) \text{ \AA}$ and the structure determined on single-crystalline samples by Carim *et al.* is confirmed. In order to investigate the symmetry lowering below T_N , we have examined the extinction rule for the Bragg reflections at 78 K, and have found no superlattice reflections stronger than 10^{-5} of the fundamental reflection intensity. This indicates that the $Cmca$ symmetry holds below T_N , and that the phase transition is not driven

by lattice instability. We have carefully examined the temperature dependence of the $(0\ 0\ 2)$ intensity, and have found it essentially independent of temperature below T_N . Thus we can conclude that the growth of the $(0\ 0\ 2)$ intensity observed in the neutron experiment below T_N is of magnetic origin, as Klein *et al.* suggested previously.⁶ The atomic coordinates and isotropic thermal parameters are listed in Table I, which agree with the previous works.^{5,6}

TABLE I: Atomic coordinates and thermal parameters for $\text{Ba}_4\text{Ru}_3\text{O}_{10}$ at 300 K.

Atom Site	x	y	z	$\beta (\text{\AA}^2)$
Ba(1) 8f	0	0.23970(3)	0.11143(3)	0.0106(3)
Ba(2) 8f	0	0.53555(3)	0.13884(3)	0.0082(3)
Ru(1) 4a	0	0	0	0.0058(3)
Ru(2) 8f	0	0.87538(4)	0.14943(4)	0.0052(3)
O(1) 8e	1/4	0.3784(4)	1/4	0.0118(13)
O(2) 8f	0	0.0360(4)	0.1521(4)	0.0061(12)
O(3) 16g	0.2736(6)	0.3901(2)	0.0347(3)	0.0072(8)
O(4) 8f	0	0.7285(5)	0.1482(4)	0.0141(14)

Table II lists the temperature dependence of the lattice parameters, reliability factors, and the Ru-O and Ru(1)-Ru(2) distances for Sample1 and Sample2. All the refinements lead to reliability factors R_1 (all data) with a precision better than 0.02. At 300 K, the Ru(1)-Ru(2) distance is determined to be $2.5576(6) \text{ \AA}$. This is significantly shorter than that of the ruthenium metal (2.65 \AA), and decreases with decreasing temperature, which implies that the hybridization of the Ru $4d$ orbitals becomes stronger at low temperatures.

Figure 2 shows the temperature dependence of the cell parameters using the data for Sample1 and Sample2 together with the neutron data in Ref. 6, where all of the cell parameters decrease with decreasing temperature. The b axis decreases by 0.2 % between 300 and 78 K for Sample1, which is larger than the change in the other axes. The parameters for Sample1 and Sample2 are 1.7 % smaller than the neutron data, which could come from delicate difference in chemical composition between the polycrystalline sample and single crystals and in the measurements between x-ray structural analysis and neutron powder diffraction. The lattice volume differs only by 0.05 % between Sample1 and Sample2 at 78 K.

Figure 3 shows the temperature dependence of the relative change in the Ru-O distances $\Delta R/R_{300}$ together with the temperature evolution of volume shrinkage plotted using the dashed lines. Here, ΔR is a change of the Ru-O distance from 300 K and R_{300} is the Ru-O distance at 300 K. The Ru(1)-O(2) and Ru(1)-O(3) values roughly lie on the dashed line. In contrast, the Ru(2)-O distances plunge under the dashed line, and in particular, the Ru(2)-O(2) and Ru(2)-O(4) distances for Sample2 significantly decrease below 150 K. This indicates that the volume of the Ru(2)O₆ octahedron shrinks more remarkably than the thermal average, while that of the Ru(1)O₆ octahedron is weakly dependent on temperature.

We should emphasize that the mean Ru-O distance of $\text{Ba}_4\text{Ru}_3\text{O}_{10}$ is exceptionally long. As listed in Table II, the mean distances of Ru(1)-O and Ru(2)-O are $2.028(4)$ and

TABLE II: Temperature dependence of structure analysis data and selected inter atomic distances for Sample1 and Sample2.

		Sample1				Sample2		
		300 K	218 K	93 K	78 K	133 K	113 K	78 K
Cell parameters(Å)	<i>a</i>	5.7740(5)	5.7729(6)	5.7661(8)	5.7606(6)	5.7653(4)	5.7646(5)	5.7593(5)
	<i>b</i>	13.2571(10)	13.2472(10)	13.2326(11)	13.2284(12)	13.2322(13)	13.2291(13)	13.2223(15)
	<i>c</i>	13.0649(9)	13.0597(9)	13.0529(11)	13.0473(13)	13.0556(11)	13.0560(12)	13.0498(11)
Volume (Å ³)		1000.07(13)	998.74(15)	995.94(18)	994.25(17)	995.98(15)	995.66(16)	993.76(16)
No. of independent reflections		559	560	561	562	2195	2196	2191
Goodness of Fit		0.820	0.836	0.837	0.859	0.944	0.928	0.99
Reliability factor <i>R</i> 1	($F_0 > 4\sigma(F_0)$)	0.018	0.0171	0.0179	0.0180	0.0189	0.0178	0.0182
	(all data)	0.0188	0.0181	0.0188	0.0188	0.0193	0.0183	0.0185
Reliability factor <i>wR</i> 2		(all data)	0.0843	0.0857	0.0862	0.0883	0.1034	0.1081
Bond length (Å)								
Ru(1)-O(2)		2.043(5)	2.040(4)	2.043(5)	2.044(6)	2.044(2)	2.043(2)	2.040(3)
Ru(1)-O(3)		2.021(3)	2.013(3)	2.025(4)	2.025(4)	2.0211(15)	2.0211(15)	2.0245(16)
Ru(2)-O(1)		1.9523(4)	1.9517(4)	1.9511(4)	1.9502(4)	1.95008(17)	1.95057(19)	1.94951(19)
Ru(2)-O(2)		2.130(5)	2.121(5)	2.117(5)	2.126(6)	2.113(2)	2.113(2)	2.107(3)
Ru(2)-O(3)		2.010(4)	2.011(3)	2.006(4)	2.007(4)	2.0109(15)	2.0104(15)	2.0069(16)
Ru(2)-O(4)		1.948(7)	1.951(6)	1.944(6)	1.943(7)	1.926(2)	1.924(2)	1.927(3)
Ru(1)-Ru(2)		2.5576(6)	2.5560(6)	2.5530(6)	2.5505(6)	2.5551(3)	2.5543(3)	2.5522(3)
Ru(1)-O mean		2.028(4)	2.022(4)	2.031(5)	2.031(5)	2.029(2)	2.028(2)	2.030(2)
Ru(2)-O mean		2.000(4)	2.000(3)	2.000(3)	1.997(4)	1.993(2)	1.993(2)	1.991(2)

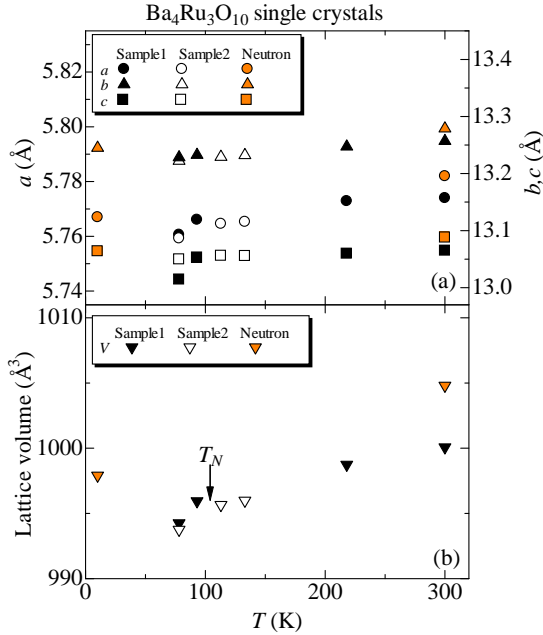


FIG. 2: (Color online) (a) The lattice constant *a* (left scale), *b*, and *c* (right scale) as a function of temperature. (b) The unit cell volume of Ba₄Ru₃O₁₀ as a function of temperature. Neutron data on the polycrystalline samples are also shown.⁶

2.000(4) Å at 300 K, respectively. These values are significantly larger than the mean Ru-O distance in Sr₂RuO₄ and Ca₂RuO₄ (1.98-1.99 Å),⁹ which implies that the formal Ru valence in the title compound is lower than 4+ on the basis of a bond-valence sum calculation.¹⁰ We should further note that Ru(1)-O is longer than Ru(2)-O, meaning that the formal valence of Ru(1) is lower than that of Ru(2).

Based on the analyzed structure, we evaluate the formal Ru valence using the bond valence sum method, where we use 1.834 Å as a standard distance *d*₀ of Ru⁴⁺ ion.¹⁰ The formal valences of Ru(1) and Ru(2) are calculated to be 3.55 and 3.88 at 300 K, respectively, as shown in Fig. 4, as was already expected from the long Ru-O distances discussed above. A valence lower than 4+ is directly related to the longer Ru-O distances, possibly because the intra-trimer Ru ions push the intervening oxygen ions away by coming closer to each other. More importantly, the valence difference of 0.33 between the inner and outer Ru is far larger than what is commonly observed in the charge-ordered oxides, e.g., Pr_{0.6}Ca_{0.4}MnO₃¹¹ and Fe₃O₄.¹² This implies that the degree of the charge disproportionation can be much larger, meaning that it may exceed +*e*. If different *d*₀ distances are assumed for the Ru(1) and Ru(2) sites as was done for LiMn₂O₄,¹³ the valences of Ru(1) and Ru(2) can be evaluated to be 2.99+ (*d*₀ = 1.77 Å for Ru³⁺) and 4.64+ (*d*₀ = 1.90 Å for Ru⁵⁺) respectively.¹⁴ These valences agree with our proposed model based on a localized picture of *t*_{2g} electrons (See the discussion below).

Let us consider the electronic states of the Ru₃O₁₂ trimer. Very recently, two groups were independently calculated the

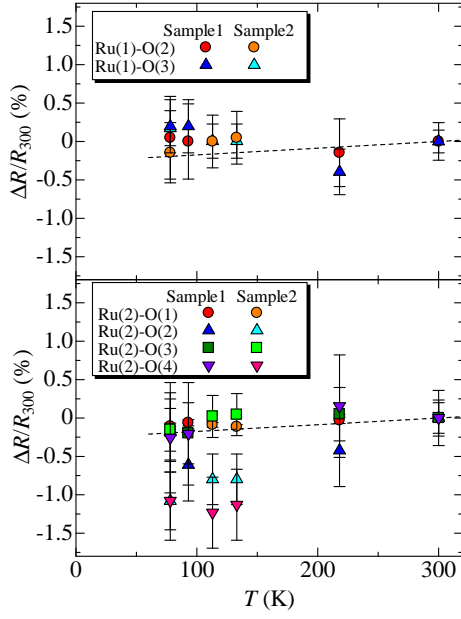


FIG. 3: (Color online) The relative change in the Ru-O distances of $\text{Ba}_4\text{Ru}_3\text{O}_{10}$ as a function of temperature. Dashed lines are the volume shrinkage from 300 K. $\Delta R/R_{300}$ is referred to the text.

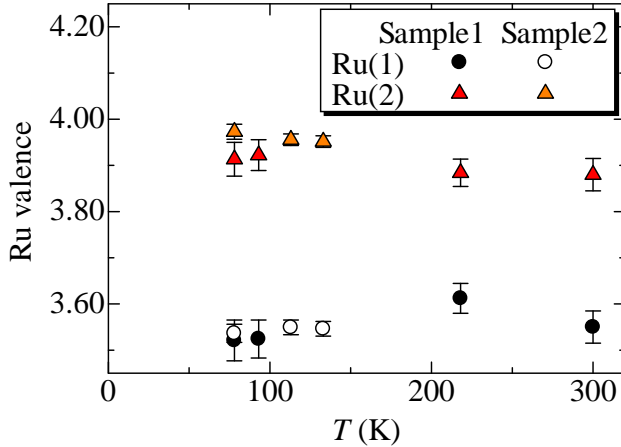


FIG. 4: (Color online) The Ru(1) and the Ru(2) valences of $\text{Ba}_4\text{Ru}_3\text{O}_{10}$ as a function of temperature.

electronic states of $\text{Ba}_4\text{Ru}_3\text{O}_{10}$ ^{15,16} The two papers discussed the electronic states of the title compound from an itinerant picture using the density functional theory. We will start from the electronic states of an isolated Ru_3O_{12} trimer, and then introduce a small inter-trimer transfer. This approach may not be exact, but can give us intuitive insight for the electronic states and the electronic transition of $\text{Ba}_4\text{Ru}_3\text{O}_{10}$. As shown in the left side of Fig. 5(a), the four d electrons in the Ru^{4+} ion

partially occupy the t_{2g} orbitals to make the low-spin state. At first, we consider that the octahedra in each Ru site are compressed along the Ru-Ru direction, and t_{2g} orbitals split into a_{1g} and e'_g orbitals with a crystal-field splitting of Δ as is schematically shown in the right side of Fig. 5 (a). We then consider the formation of molecular orbital for all the orbitals. We set the quantization z axis to be parallel to the Ru-Ru direction. Since one of the orbitals in each Ru site is extended to the z axis at a 180-degree angle of Ru(2)-Ru(1)-Ru(2), the a_{1g} orbitals form a strong σ bonding. By neglecting the correlation effects, we can construct bonding (B), non-bonding (NB) and anti-bonding (AB) orbitals. We also take account of the e'_g orbitals with δ bonding.

Figure 5(b) shows the electronic states in three Ru ions without Ru-Ru transfer energies. We use the simplest Hamil-

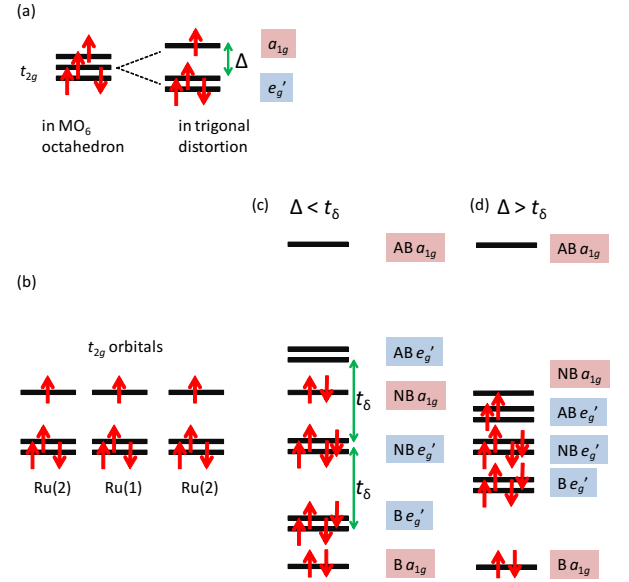


FIG. 5: (Color online) (a) Splitting t_{2g} orbital in a_{1g} and e'_g orbitals caused by trigonal distortion in a trimer. (b) t_{2g} orbitals in the three Ru sites. The energy levels in the trimer (c) for $\Delta < t_\delta$ and (d) for $\Delta > t_\delta$. The a_{1g} and e'_g orbitals hybridize to form the anti-bonding (AB), non-bonding (NB) and bonding (B) orbitals.

tonian given by^{15,16}

$$H = \begin{bmatrix} 0 & t_i & 0 \\ t_i & 0 & t_i \\ 0 & t_i & 0 \end{bmatrix} \quad (i = \sigma, \delta). \quad (1)$$

Then molecular orbital is expressed by $\Psi_{AB} = (\phi_1 - \sqrt{2}\phi_2 + \phi_3)/2$, $\Psi_{NB} = (\phi_1 - \phi_3)/\sqrt{2}$, and $\Psi_B = (\phi_1 + \sqrt{2}\phi_2 + \phi_3)/2$, where ϕ_1 , ϕ_2 , and ϕ_3 are the orbitals in the left Ru(2), Ru(1), and right Ru(2) ions, respectively. The energy splitting is given as $\pm t_\sigma$ for the a_{1g} orbital, and $\pm t_\delta$ for the e'_g orbital.

Let us first consider $\Delta < t_\delta$. The highest occupied orbital is the fully-filled NB a_{1g} orbital. This electronic configuration is, however, nonmagnetic, which is in a serious contradiction to the experimental fact that Ru(2) is magnetic.⁶ The valence

of Ru(1) and Ru(2) site are 5+ and 3.5+, because the NB orbitals have no weight at the Ru(1) site, as was indicated in the previous works.^{15–17} This estimation also disagrees with the BVS calculation result that the Ru(1) is of lower valence. When $\Delta > t_\delta$, the highest occupied state is AB e'_g , where the spins of the two electrons are aligned in parallel. In this case, however, the magnetic moment exists in the Ru(1) site, which disagrees with the neutron experiment.

In order to modify the model in Fig. 5, we retain the

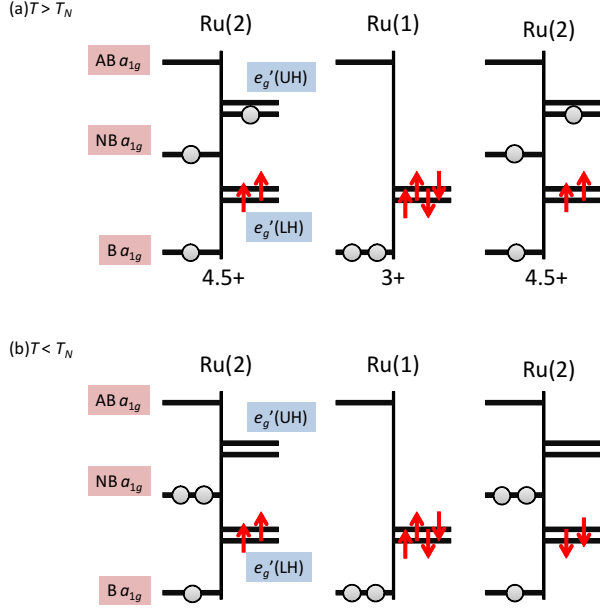


FIG. 6: (Color online) Proposed energy diagram for the Ru trimer in Ba₄Ru₃O₁₀. (a) $T > T_N$ and (b) $T < T_N$. The energy levels for the molecular orbitals of the a_{1g} orbitals are drawn in the left, and those for the e'_g orbitals in the right. A grey circle represents 0.5 electron and an arrow represents a localized electron. (See text)

B, NB and AB a_{1g} orbitals, but introduce the upper Hubbard (UH) and lower Hubbard (LH) e'_g orbitals. This is based on the fact that the magnetic susceptibility of Ba₄Ru₃O₁₀ above T_N suggests an existence of a local moment. We also note that similar local moments are suggested in some Ru oxides such as Ba₃CoRu₂O₉¹⁸ and Ba₃BiRu₂O₉,¹⁹ where a_{1g} and e'_g orbitals can act different roles.²⁰ To express the a_{1g} molecular orbitals and the Hubbard-split e'_g orbitals simultaneously, we draw energy levels in an unconventional way in Fig. 6. As shown in Fig. 6, each Ru ion shows the a_{1g} levels in the left and the e'_g levels in the right. While the energy diagram for the e'_g levels follows the convention, that for the a_{1g} levels represents the weight for the wave functions of ϕ_1 , ϕ_2 , and ϕ_3 . Let us focus the bonding a_{1g} orbital, which is expressed as $(\phi_1 + \sqrt{2}\phi_2 + \phi_3)/2$. Thus the weight for the 1, 2, 3 sites are 0.5e, 1.0e and 0.5e, respectively. We denote this situation by using gray circles in Fig. 6. Similarly, the half-filled NB a_{1g} orbital is expressed as $(\phi_1 - \phi_3)/\sqrt{2}$, which corresponds to 0.5e in the Ru(2) sites, as shown in Fig. 6(a).

To understand the charge disproportionation within the

trimer, let us count the number of electrons in the Ru(1) and Ru(2) ions. As discussed above, the a_{1g} molecular orbitals give 1.0e for each Ru site. Owing to the deep level of the bonding a_{1g} orbital, the center of gravity in the density of states for Ru(1) shifts to lower energies, which implies that a finite charge should be transferred from Ru(2) to Ru(1).¹⁵ Assuming that a charge of 0.5e is transferred from Ru(2) UH e'_g orbitals to Ru(1) e'_g orbital (i.e., Ru(1) is 3+ and Ru(2) is 4.5+), the four electrons fully occupy the e'_g levels in the Ru(1) site to let the Ru(1) ion be nonmagnetic as shown in Fig. 6(a). On the other hand, 0.5e, 0.5e and 2.0e occupy the levels of NB a_{1g} , UH e'_g and LH e'_g in the Ru(2) site, respectively. At first sight, the highest occupied level of the UH e'_g orbitals in Fig. 6(a) is unstable against the half-filled NB a_{1g} orbital. We think that this instability will be removed by introducing an inter-trimer hopping to form the a_{1g} and e'_g bands. Figure 6(a) captures some essential features given in Refs. 13 and 14. The charge disproportionation in Ref. 13 is comparable with ours, and the charge distribution between a_{1g} and e'_g in Ref. 14 is similar to ours.

Based on this self-disproportionation picture, we can explain the following experimental facts from the above mentioned intra-trimer charge disproportionation of Ru³⁺/Ru^{4.5+}: (i) The lower Ru(1) valence reasonably close to 3+, (ii) The valence difference larger than that in Mn³⁺/Mn⁴⁺ ordered materials suggested from the bond-valence-sum calculation, (iii) the nonmagnetic Ru(1) site and the magnetic Ru(2) site, (i v) no charge gap above T_N , (v) nonmetallic resistivity above T_N implying narrow conduction bands formed by the NB a_{1g} and the localized UH e'_g bands, and (vi) the small positive thermopower and negative Hall coefficient suggesting multiband conduction. However, it is fair to point out some open issues. One is how to directly observe the large difference of valence between Ru(1) and Ru(2) site. Second one is how to observe the Hubbard-split e'_g orbitals. Optical or photoemission measurements are needed to explore the electronic states.

We have further found that the charge disproportionation develops with decreasing temperature. Figure 4 shows the formal Ru valence plotted as a function of temperature. Mirroring the weak temperature dependence of the Ru(1)-O distances, the Ru(1) valence is nearly independent of temperature. In contrast, the significant shrinkage of the Ru(2)-O(2) and Ru(2)-O(4) distances results in the increase of the Ru(2) valence from 300 down to 78 K. These results indicate that the charge disproportionation in this compound does not arise simply from a band picture, but from some cooperative motion of 4d electrons. Although the valence change is so smooth below and above T_N , the valence difference at 78 K reaches 0.45, which is anomalously large in comparison with other charge-ordered materials.

We do not yet understand the mechanism of the 105 K transition from the paramagnetic metal to the antiferromagnetic insulator, but will try to discuss some possible scenarios on the basis of the electronic states discussed above. We can exclude possibilities of charge and spin density waves, because these phases accompany the translational symmetry breaking.²¹ For the same reason, we can also exclude a possibility of the Slater insulator.²² One possibility is driven by the

short-range magnetic order. In the title compound, a broad maximum around 200 K in the susceptibility implies that a short-range antiferromagnetic correlation develops below 200 K, which has been analyzed in terms of spin dimer above T_N by Radtke *et al.*¹⁶ We propose a possible electron configuration below T_N in Fig. 6(b). Assuming the Hund coupling between the NB a_{1g} and the e'_g electrons, we expect that the electron spin in the NB a_{1g} orbital tends to polarize in parallel to the spin in the e'_g orbitals. However, since the spins of the Ru(2) sites are ordered in antiparallel, the spin in the NB a_{1g} orbital is frustrated. To relieve this frustration, we propose that a charge of 0.5e will be transferred from the UH e'_g orbitals to the NB a_{1g} orbital to let the NB a_{1g} be nonmagnetic with opening the charge gap between the NB a_{1g} orbital and the UH e'_g orbitals. In this respect, this electronic phase transition can be viewed as an orbital ordering transition.

Finally, we should emphasize that the Ru valence difference observed here is intrinsic to the hexagonal-perovskite ruthenates. In the related ruthenate BaRuO₃ composed of similar trimers,²³ the calculated partial density of states²⁴ and the neutron diffraction²⁵ have revealed that the valence of the Ru(1) site is lower than 4+. A vitally important difference is that a phase transition does not occur, but a pseudogap is observed in the optical conductivity and the charge transport in BaRuO₃.^{26,27} We think that the origin of the pseudogap is the intra-trimer charge disproportionation discussed in this article, and that the absence of the phase transition should be ascribed to the different trimer network from Ba₄Ru₃O₁₀.

IV. SUMMARY

We have successfully grown high-quality Ba₄Ru₃O₁₀ single crystals, and have solved the crystal structure with a reli-

ability factor better than 2% at all the temperatures from 78 to 300 K through x-ray crystal analysis. This ruthenate is orthorhombic with space group *Cmca* (space group No. 64) at all temperatures, and no symmetry breaking is detected below the antiferromagnetic transition of 105 K. We have further found that the Ru-O distances are anomalously long, and that the formal Ru valence is smaller than 4+ according to the bond-valence-sum calculation. Most remarkably, a large charge disproportionation of 0.45e within the Ru₃O₁₂ trimer is obtained at 78 K, which is ascribed to the strong hybridization of the Ru a_{1g} orbital. We have explained the experimental results on the basis of the solved structure, and proposed a model from a localized picture of t_{2g} electrons.

Acknowledgements

The authors gratefully thank Division of Instrumental Analysis, Okayama University for the x-ray measurements, G. Radtke for the discussions about band calculations, and H. Nakao for useful discussions. This work was partially supported by the Grant-in-Aid(No. 23110714). One of authors(T. Igarashi) was supported by Program for Leading Graduate Schools" Integrative Graduate Education and Research in Green Natural Sciences", MEXT, Japan.

* Electronic address: igarashi.taichi@b.mbox.nagoya-u.ac.jp

† Visiting professor in the Department of Physics, Nagoya University

¹ S. Nakatsuji, S. Ikeda, and Y. Maeno: J. Phys. Soc. Jpn. **66** (1997) 1868.

² Y. Maeno, H. Hashimoto, K. Yoshida, S. Nishizaki, T. Fujita, J. Bednorz, and F. Lichtenberg: Nature **372** (1994) 532.

³ J. P. Carlo, T. Goko, I. M. Gat-Malureanu, P. L. Russo, A. T. Savici, A. A. Aczel, G. J. MacDougall, J. A. Rodriguez, T. J. Williams, G. M. Luke, C. R. Wiebe, Y. Yoshida, S. Nakatsuji, Y. Maeno, T. Taniguchi, and Y. J. Uemura: Nat. Mater. **11** (2012) 323.

⁴ C. Dussarrat, F. Grasset, R. Bontchev, and J. Darriet: J. Alloys and Compd. **233** (1996) 15.

⁵ A. H. Carim, P. Dera, L. W. Finger, B. Mysen, C. T. Prewitt, and D. G. Schlom: J. Solid State Chem. **149** (2000) 137.

⁶ Y. Klein, G. Rousse, F. Damay, F. Porcher, G. André, and I. Terasaki: Phys. Rev. B **84** (2011) 054439.

⁷ G. M. Sheldrick: Acta Crystallogr., Sect. A **64** (2008) 112.

⁸ C. Kabuto, S. Akine, T. Nemoto, and E. Kwon: J. Cryst. Soc. Jpn. **51** (2009) 218 [in Japanese].

⁹ M. Braden, G. André, S. Nakatsuji, and Y. Maeno: Phys. Rev. B

58 (1998) 847.

¹⁰ N. E. Brese and M. O'Keeffe: Acta Crystallogr. Sect. B **47** (1991) 192.

¹¹ A. Daoud-Aladine, J. Rodríguez-Carvajal, L. Pinsard-Gaudart, M. T. Fernández-Díaz, and A. Revcolevschi: Phys. Rev. Lett. **89** (2002) 097205.

¹² M. S. Senn, J. P. Wright, and J. P. Attfield: Nature **481** (2012) 173.

¹³ J. Rodríguez-Carvajal, G. Rousse, C. Masquelier, and M. Hervieu: Phys. Rev. Lett. **81** (1998) 4660.

¹⁴ R. Allmann: Monatsh. Chem. **106** (1975) 779.

¹⁵ S. Streltsov and D. Khomskii: Phys. Rev. B **86** (2012) 064429.

¹⁶ G. Radtke, A. Saúl, Y. Klein, and G. Rousse: Phys. Rev. B **87** (2013) 054436.

¹⁷ B. E. Bursten, F. A. Cotton, and A. Fang: Inorg. Chem. **22** (1983) 2127.

¹⁸ H. D. Zhou, A. Kiswandhi, Y. Barlas, J. S. Brooks, T. Siegrist, G. Li, L. Balicas, J. G. Cheng, F. Rivadulla, Phys. Rev. B **85** (2012) 041201.

¹⁹ W. Müller, M. Avdee, Q. Zhou, A. J. Studer, B. J. Kennedy, G. J. Kearley, C. D. Ling, Phys. Rev. B **84** (2011) 220406.

²⁰ S. V. Streltsov: cond-mat/1306.3333.

²¹ G. Grüner: Rev. Mod. Phys. **60** (1988) 1129.

- ²² Y. G. Shi, Y. F. Guo, S. Yu, M. Arai, A. A. Belik, A. Sato, K. Yamaura, E. Takayama-Muromachi, H. F. Tian, H. X. Yang, J. Q. Li, T. Varga, J. F. Mitchell, and S. Okamoto: Phys. Rev. B **80** (2009) 161104.
- ²³ P. C. Donohue, L. Katz, and R. Ward: Inorg. Chem. **4** (1965) 306.
- ²⁴ C. Felser and R. J. Cava: Phys. Rev. B **61** (2000) 10005.
- ²⁵ A. Santoro, I. N. Sora, and Q. Huang: J. Solid State Chem. **151** (2000) 245.
- ²⁶ Y. Klein and I. Terasaki: Phys. Rev. B **76** (2001) 165105.
- ²⁷ T. W. Noh, Y. S. Lee, J. S. Lee, K. W. Kim, J. Yu, G. Cao, J. E. Crow, M. K. Lee, and C. B. Eom: Physica C **364-365** (2001) 480.